

Description of proton-rich nuclei in the $A \approx 20$ region within the Gamow shell model

N. Michel^{1,2,*}, J. G. Li³, F. R. Xu³ and W. Zuo^{1,2,†}

¹*Institute of Modern Physics, Chinese Academy of Sciences, Lanzhou 730000, China*

²*School of Nuclear Science and Technology, University of Chinese Academy of Sciences, Beijing 100049, China*

³*School of Physics, and State Key Laboratory of Nuclear Physics and Technology, Peking University, Beijing 100871, China*



(Received 18 September 2019; published 3 December 2019)

The Gamow shell model is utilized to describe nuclear observables of the weakly bound and resonance isotonic states of ^{16}O at the proton drip-line. It is hereby shown that the presence of continuum coupling leads to complex Coulomb contributions in the spectrum of these isotones. The necessity to include the effects of three-body forces, either by a direct calculation or by adding an A dependence to the nucleon-nucleon interaction, already noticed in other theoretical models, is pointed out. It is also demonstrated that our approach is predictive for reaction observables.

DOI: [10.1103/PhysRevC.100.064303](https://doi.org/10.1103/PhysRevC.100.064303)

I. INTRODUCTION

Accelerators of the new generation, based on the use of radioactive ion beams, have allowed us to study nuclei up to the proton and neutron drip-lines [1–4]. The location of the neutron drip-line is not well known experimentally, because the heaviest drip-line neutron-rich nuclei to have been synthesized in accelerators are ^{31}F and ^{40}Mg [5–8]. Conversely, the proton drip-line has been reached experimentally up to $Z \approx 90$ since already more than a decade [9]. Nevertheless, due to the very large Coulomb barrier for large Z , it is difficult to generate drip-line nuclei beyond $Z = 90$ [9]. Indeed, to our knowledge, the heaviest proton drip-line nucleus to have been synthesized in the recent years is ^{219}Np , for which $Z = 93$ [10]. Moreover, unbound nuclei close to the proton drip-line bear a very long lifetime, often of a few milliseconds [3], so that it is not always clear whether the proton drip-line has been crossed during an experiment [9]. In fact, to our knowledge, the exact location of the proton drip-line is only known before aluminum, for which $Z = 13$ [9]. The production of nuclei bearing a large number of protons is also challenging in the domain of superheavies, where elements whose charge number is larger than 110 have been produced [4]. The heaviest element to date to have been synthesized in an accelerator is the $Z = 118$ element, called Oganesson from its discoverer Y.T. Oganessian [11].

Due to the large confining Coulomb barrier at the proton drip-line, proton-rich nuclei can be usually described by models devised for well-bound nuclei, such as shell model based on a basis of harmonic-oscillator states (HO-SM) [12–14]. However, the proton emitters, usually found in the $A \approx 110$ –150 region and which have a very small particle-emission width, demand the use of elaborate methods to calculate their

widths precisely. The use of the two-potential method in the spherical case [15], or coupled-channel models in the nonadiabatic approach in the axially deformed case [16,17], have been seen to be very successful for that matter. In fact, very light proton-rich nuclei can bear the same unusual properties found at the neutron drip-line, in which the Coulomb interaction plays very little role. For example, the ground states of ^5Li and ^7B are very broad-resonance states, as they bear a width of about 1 MeV. While being more narrow, the ground states of ^6Be and ^8C are unbound by about 100 keV. Moreover, proton-rich nuclei at drip-lines can also sustain halos, albeit less frequently than neutron-rich nuclei [18]. Indeed, the ground states of ^8B and ^{13}N and the first-excited state of ^{17}F are one-proton halos, and that of ^{17}Ne is a two-proton halo [18]. Among the features which can develop only at the proton drip-line, one can also cite diproton emission, which has been discovered one to two decades ago [19,20]. The theoretical description of diproton emitters demands the rigorous treatment the asymptotic region. For this, the use of the shell model embedded in the continuum along with the cluster approximation has been seen to be successful because it could provide diproton emission widths close to experimental data [21]. Consequently, the variety of phenomena induced by the proximity of the proton-emission threshold shows that one has to describe precisely the asymptotic part of many-body wave functions.

For proton-rich nuclei whose number of nucleons is close to 20, the Coulomb barrier is already rather large, so that one can expect protons to be confined in general in the nuclear zone. Nevertheless, the proton-emission threshold is low therein, so that effects due to the proximity of the continuum also appear in nuclear states. Consequently, both Coulomb and continuum effects compete in proton-rich nuclei, so that continuum coupling has to be included explicitly. For this, the Gamow shell model (GSM), which incorporates both continuum coupling and internucleon correlations, is the tool of choice for this type of applications [22–24]. Indeed, the

* nicolas.michel@impcas.ac.cn

† zuowei@impcas.ac.cn

GSM has become a predictive tool of experimental interest for structure and reaction observables of nuclei at the drip-line because it has been used to analyze the $^{14}\text{O}(p, p)$ elastic reaction cross section [25], ^{25}O spectroscopy [26], and the newly discovered $^{20,21}\text{B}$ isotopes at the neutron drip-line [27]. The GSM has also been introduced successfully to the use of realistic Hamiltonians, in a no-core approach [28], or in a core + valence nucleons picture, using an effective Hamiltonian calculated from the full Q -box folded-diagram renormalization [29]. The equation of motion method used along with Gamow states has also been introduced via the in-medium similarity renormalization-group method [30].

As a consequence, GSM is well suited to study the proton-rich isotonic systems of ^{16}O , which will be the object of this paper. These isotones are interesting for several reasons. First, they are the mirror systems of the neutron-rich isotopes of the oxygen chain, which is being intensively studied experimentally [26,31–33] and theoretically [23,34,35]. Consequently, one can directly consider its isospin-breaking features because continuum coupling is known to break isospin symmetry, in particular with the so-called Thomas-Ehrman shift [36,37]. Moreover, as noticed in Ref. [13,38], an important contribution coming from three-body forces of a few MeV has been seen to be necessary to properly reproduce the experimentally known binding energies at either the proton or neutron drip-line. Three-body forces can be rather precisely mimicked by a two-body effective Hamiltonian at the neutron drip-line because the latter method only leads to an overbinding of 500 keV for ^{28}O in Ref. [23]. However, an A dependence of the Hamiltonian was seen to be necessary in Ref. [25] to reproduce the $^{14}\text{O}(p, p)$ elastic reaction cross section while using the same Hamiltonian structure. It thus appeared that approximating three-body forces by a simple two-body operator might not be as precise at the proton drip-line as at the neutron drip-line. Finally, the treatment of the Coulomb Hamiltonian can be analyzed rigorously with the GSM. Indeed, the method of Ref. [39] allows us to include the Coulomb Hamiltonian almost exactly, on the one hand, and the correlations induced by the Coulomb interaction in the asymptotic region are present as well due to the inclusion of continuum coupling, on the other hand. In particular, one can test the precision of the formula usually used for Coulomb energy based on the isobaric multiplet mass equation (IMME) [40–42].

This paper is constructed as follows: We first recall the basic features of the GSM by insisting on the issues raised by the presence of the Coulomb interaction in the asymptotic region. We then describe the Hamiltonians used to describe the studied isotones of ^{16}O , where a core + valence protons approach will be considered. We compare two different interactions: the first one being local, of the Furutani-Horiuchi-Tamagaki (FHT) type [43,44], and the second one nonlocal, as issued from effective-field theory (EFT) [45]. We then show the calculated energy spectra of the proton-rich isotones of ^{16}O , the calculated Coulomb contributions in their ground states and in the excited states of ^{18}Ne and ^{20}Mg , using both GSM and IMME frameworks, and the calculation of the elastic-scattering cross sections of $^{18}\text{Ne}(p, p)$. The latter calculation will allow us, in particular, to state the predictive power of our formalism because the considered cross sections do not enter

the fitting procedure used to build the used Hamiltonians. The conclusion of this work will be made afterwards.

II. THEORETICAL MODEL

The theoretical model used is that of the GSM (see Ref. [24] for a review and Refs. [23,26,46–50] for recent applications of the model). It is a configuration-interaction framework based on the one-body Berggren basis [51]. The Berggren basis is generated by a finite-range potential and possesses bound, resonance, and scattering states:

$$\sum_n |n\rangle \langle n| + \int_{L^+} |k\rangle \langle k| dk = 1, \quad (1)$$

where $|n\rangle$ is a resonant state, and L^+ is a contour in the complex-momentum plane, starting from $k = 0$, going to $k \rightarrow +\infty$, and encompassing the resonance states of the finite sum (see Fig. 1). Consequently, the Berggren basis is the complex extension of the real-energy completeness relation of Newton [52], consisting of bound states and of a continuum of real-energy scattering states. Contrary to the Newton completeness relation, with which only localized states can be expanded, the Berggren basis can expand resonance states. Equation (1) is one dimensional, i.e., it is built from the one-body states of a fixed partial wave. Thus, the three-dimensional completeness relation at the one-body level is recovered by considering Eq. (1) for all possible partial waves. The many-body completeness relation follows by constructing Slater determinants from the bound, resonance, and scattering Berggren one-body basis states [24]. From a numerical point of view, the L^+

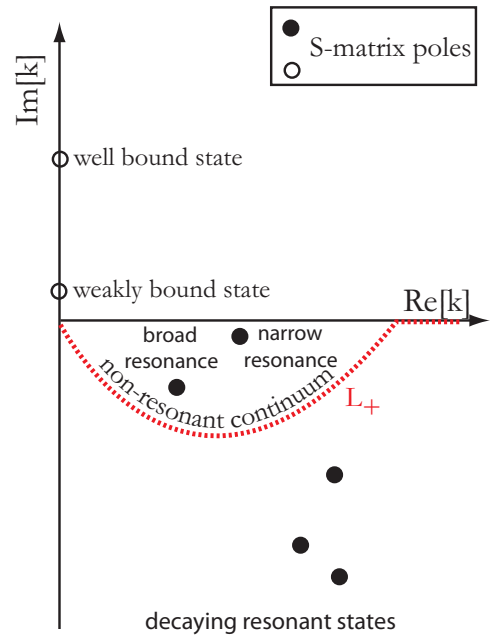


FIG. 1. Depiction of the Berggren basis in the complex-momentum plane for a fixed partial wave. Typical complex momenta of bound, narrow, and broad-resonance states, i.e., S -matrix poles, are provided. The L_+ contour of scattering states encompasses the S -matrix poles of interest. Figure taken from Ref. [28].

contour is discretized with a Gauss-Legendre quadrature in order to obtain an eigenproblem similar to that of HO-SM [24]. It has been checked that 15–45 states per contour are necessary to have converged results. The Hamiltonian is represented by a complex symmetric matrix, which must be diagonalized. This is handled efficiently with the complex symmetric extension of the Jacobi-Davidson method [53], where one takes advantage of the relatively small coupling to the continuum to have a fast convergence of eigenstates. While the full configuration space is extremely large, reasonably small dimensions are obtained by truncating the GSM space with two scattering states occupied at most in the continuum, which we denote $2p$ - $2h$. It is possible to lift space truncation if one uses the density renormalization-group method [54,55] because the many-body basis of Slater determinants is hereby replaced by a correlated many-body basis issued from the diagonalization of the density matrix. However, continuum coupling is usually small in the $A \approx 20$ region [56], so that $2p$ - $2h$ truncations are sufficiently precise.

The presence of the Coulomb Hamiltonian generates additional difficulties when using a Berggren basis of proton states. First, the asymptote of one-body basis states is that of Coulomb wave functions, whose structure is more complex than that of the Hankel functions occurring in the neutron case. The use of the computational methods of Ref. [57] are hereby necessary to precisely calculate bound, resonance, and scattering states with a Coulomb wave-function asymptote. Second, the Hamiltonian is of infinite range due to the Coulomb Hamiltonian. To deal with this situation, we use the method developed in Ref. [58]. For this, one separates the Coulomb Hamiltonian into a one-body-potential part, whose asymptote is in $(Z-1)/r$, to which a finite-range residual two-body part is added. The residual two-body Coulomb part is expanded with a basis of HO states, so that it can be treated in a standard fashion by using the Talmi-Brody-Moshinsky transformation [59,60]. The one-body potential part of the Coulomb Hamiltonian can be directly inserted in the basis-generating potential. Its treatment is then exact because it is done at basis level. However, one cannot use this method if we consider observables involving nuclear eigenstates of different charges, as will be the case for the $^{18}\text{Ne}(p, p)$ cross sections. Indeed, in this case, the one-body-potential part generates infinite matrix elements using a Berggren basis. The solution to this problem, detailed in Ref. [39], consists in replacing the latter infinite matrix elements by large but finite matrix elements, depending on the used discretization for the L^+ contour (see Fig. 1). Consequently, the GSM can be used without problems with proton Berggren basis states.

The GSM approach used is that of a core + valence protons picture. The core used is that of an ^{16}O core, which is mimicked by a Woods-Saxon (WS) potential. All partial waves up to $\ell = 3$ are taken into account. As the centrifugal barrier increases quickly with orbital angular momentum, the effect of the associated partial waves on wave-function asymptotes is negligible. Hence, we use the Berggren basis for spd partial waves, whereas f partial waves are represented by a basis of harmonic-oscillator states. Two different residual nuclear proton-proton interactions have been considered. The

TABLE I. The optimized parameters of the FHT interaction consist of central (V_c^S), spin-orbit (V_{ls}^S), and tensor (V_T^S) coupling constants [47]. $S = 0, 1$ is the spin of the two protons.

Parameter	V_c^1	V_c^0	V_{ls}^1	V_T^1
Value	−2.00	−7.73	17.86	−56.79

first one is that of the FHT interaction, which is Gaussian based and bears central, spin-orbit, and tensor parts. Their coupling constants, written as V_c^S , V_{ls}^S , and V_T^S , respectively, are functions of the spin of the two protons, equal to $S = 0, 1$. The FHT interaction has been used in the GSM to describe the structure of light neutron-rich nuclei in the $A = 4$ – 10 region [47], to study neutron-rich oxygen isotopes [23] and to evaluate radiative capture reactions in $A = 6$ – 8 nuclei [48,49]. The second interaction is based on the EFT formalism [45]. It arises from an order-by-order expansion of contact terms in the EFT interaction, whose parameters are fitted on the experimental data associated with the structure of proton-rich nuclei [61]. The EFT interaction possesses the overall features of realistic nucleon-nucleon interactions [29] and is nonlocal in the short-range region, contrary to the FHT interaction. We will see, in fact, that the results of the EFT interaction are closer to experimental data than those provided by the FHT interaction.

A dependence on the number of nucleons has been added to the WS potential of the core and to the FHT and EFT two-body interactions. Indeed, it mimics the effect of missing three-body forces [62,63]. We will see in the next section that an A dependence of the Hamiltonian is necessary to reproduce experimental energies. The A dependence used for the Hamiltonian is standard [64,65]:

$$F_{1b} = 1 + f \left(\frac{N-Z}{A} \right), \quad (2)$$

$$F_{2b} = \left(\frac{A_{\text{core}} + 2}{A} \right)^e, \quad (3)$$

where Z , N , and A are the number of protons, neutrons, and nucleons of the nucleus, A_{core} is the number of nucleons of the core, here equal to 16, F_{1b} is the A -dependent one-body factor multiplied to the central depth of the WS potential, depending on the parameter f , and F_{2b} is the A -dependent two-body factor multiplied to the matrix elements of the effective interaction used, depending on the exponent parameter e .

The Hamiltonian parameters have been fit on the single-particle states of ^{17}F , and on the known experimental energies of the low-lying states of the $Z = 10$ – 12 isotones of ^{16}O . The f and e parameters of Eqs. (2) and (3) have been fixed to 0.043 and 0.3, respectively, when using A -dependent interactions. The parameters of the WS core potential are the same using either the FHT or EFT interactions. They consist of the diffuseness $d = 0.65$ fm, radius $R_0 = 2.98$ fm, central strength $V_0 = 56$ for $\ell = 0$, $V_0 = 58.075$ for $\ell = 1, 3$, and $V_0 = 58.003$ for $\ell = 2$, and spin-orbit strength $V_{ls} = 6.539$ for $\ell = 1, 3$ and 6.5 for $\ell = 2$. The parameters of the FHT and EFT interactions are shown in Tables I and II, respectively. The EFT parameters consist of the leading-order parameters, denoted

TABLE II. Optimized parameters of the EFT interaction at leading order (LO) and next-to-leading order (NLO), in natural units. See Ref. [45] for definitions and notations.

LO constant	C_S	C_T					
LO value	-2.46	-0.60					
NLO constant	C_1	C_2	C_3	C_4	C_5	C_6	C_7
NLO value	-0.25	0.55	-0.25	-0.29	-0.46	-0.13	-0.49

C_S for its spin-independent part, and C_T for its spin-dependent part, and of the next-to-leading-order parameters, denoted C_1, \dots, C_7 . The latter notation for constants is standard (see Ref. [45] for details). The EFT interaction is a low-momentum expansion valid for momenta much smaller than 1 GeV [45]. Therefore, following the prescription of Ref. [45], the EFT interaction is renormalized by way of a momentum-dependent regulator function $f(p, p')$:

$$V_{\text{EFT}}(\mathbf{p}', \mathbf{p}) \rightarrow V_{\text{EFT}}(\mathbf{p}', \mathbf{p})f(p', p), \quad (4)$$

$$f(p', p) = \exp \left[-\left(\frac{p'}{\Lambda}\right)^{2n} - \left(\frac{p}{\Lambda}\right)^{2n} \right], \quad (5)$$

where Λ is a cutoff energy of 300 MeV, and $n = 2, 3, 4$ according to the LO or NLO constant and a two-nucleon partial wave is considered (see Ref. [45] for details).

The fitted EFT parameters lie between 0.13 and 2.46 in absolute value, so that they follow the naturalness condition of low-energy constants, i.e., they are expected to be close to unity [45].

III. SPECTRA

The theoretical and experimental binding energies of the isotones of ^{16}O from ^{17}F to ^{22}Si are shown in Fig. 2. One can see that the Hamiltonians used separate into two parts, with one consisting of A -independent core potential and valence nucleon-nucleon interaction, and the other comprising A dependence in the parameters defining the one-body and two-body parts. While A -dependent Hamiltonians provide with a good description of experimental binding energies, A -independent Hamiltonians exhibit a very strong overbinding of energies when A increases. The discrepancy is already of a few hundred of keV for ^{19}Na and worsens along with the number of valence protons to reach around 2.5 MeV for ^{22}Si . It is also present when using both EFT and FHT interactions, where one can note that the overbinding encountered with the FHT interaction is larger than that of the EFT interaction. In fact, the only nucleus whose binding energy is well reproduced is ^{18}Ne . Such a behavior had already been noticed in Ref. [13] for the same nuclear systems. Moreover, the description of the $^{14}\text{O}(p, p)$ reaction with GSM [25], involving the unbound proton-rich nucleus ^{15}F , also demanded A -dependence in the Hamiltonian to properly account for proton-emission widths of the unbound spectra of ^{14}O and ^{15}F . Hence, it is highly probable that the need for strong three-body forces among valence nucleons or, equivalently, A -dependent

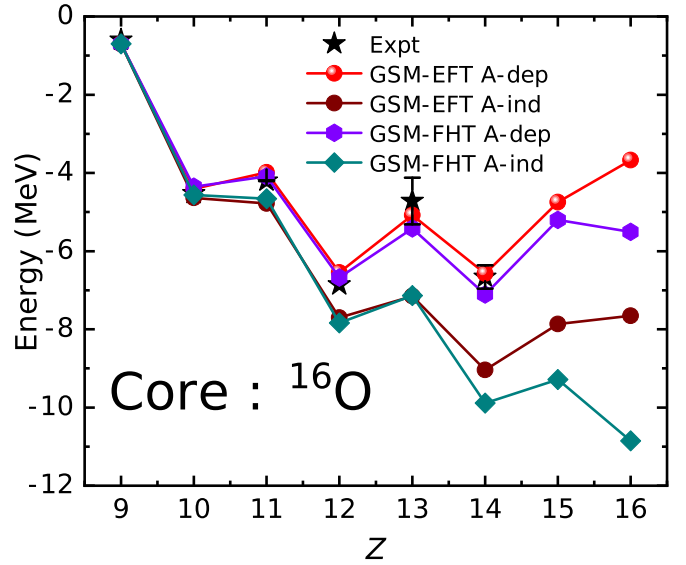


FIG. 2. Theoretical and experimental binding energies (in MeV) of the ^{16}O isotones with respect to the ^{16}O core as a function of their number of protons Z . Theoretical binding energies arise from a GSM calculation using the EFT or FHT interaction, using A -dependent interactions (A -dep) or A -independent interactions (A -ind). Experimental data are denoted by stars and are taken from AME2016 [5].

Hamiltonians, is a common feature of nuclei at the proton drip-line.

Let us compare the ground states of ^{16}O isotones to their isobaric analog states, i.e., neutron-rich oxygen isotopes, by replacing valence protons by valence neutrons. In order for the oxygen chain to be well reproduced with realistic interactions, three-body forces must be included for energy saturation to occur at the neutron drip-line [34]. Nevertheless, three-body forces can usually be mimicked by an equivalent phenomenological two-body interaction at the neutron drip-line. Indeed, using a WS potential + A -independent FHT interaction with the GSM in this region has been noticed to be only responsible for an overbinding of the ground state of ^{28}O close to 500 keV [23]. Added to that, the isobaric analog states of the ^{16}O isotones bearing $A = 17$ – 22 nucleons, consisting of 17 – ^{22}O , can be very well reproduced with a phenomenological two-body interaction, in the HO-SM [38] or in the GSM [56].

One observes that the saturation occurring at the neutron drip-line of oxygen isotopes does not exist in corresponding isotones. A strong odd-even staggering continues instead to develop therein even well after the proton drip-line, attained with ^{19}Na . More precisely, the experimental binding energies of oxygen isotopes differ by about 500 keV at the neutron drip-line, whereas they can differ by 2–3 MeV in proton-rich isotones [66]. The occurring strong odd-even staggering could be explained if protons are sufficiently localized in the nuclear zone because they could generate sizable pairing energy in this situation. This assumption can be considered by calculating the proton radial densities of the studied ground states. One can note that densities are complex for resonance states because these eigenstates have a complex energy. However, their imaginary part is small compared with their real part in

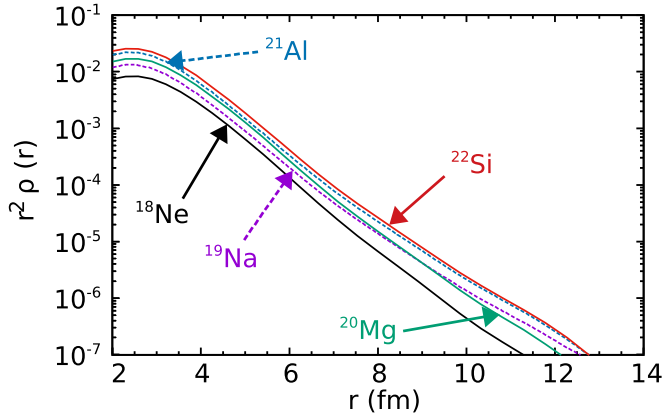


FIG. 3. Radial densities multiplied by radius squared, denoted $r^2\rho(r)$, of the ground states of the ^{16}O isotones for $A = 18$ – 22 as a function of the radius r (in fm). Even and odd isotones are represented with solid and dashed lines, respectively, and are indicated by arrows.

our calculations, so we only consider real parts when dealing with densities in this paper. It happens that proton radial densities decay rapidly for all isotones, even if they are unbound (see Fig. 3). In fact, the density of resonance states will start increasing at a radius larger than 14 fm (see Fig. 3). Therefore, one can consider that all many-body wave functions behave as bound states for $r < 14$ fm. When using a basis of harmonic-oscillator states, as in Ref. [13], this phenomenon might be seen as arising only from the well-bound character of the basis, artificially localizing many-body wave functions. As continuum coupling is exactly taken into account in the GSM, the asymptotes of many-proton systems are precisely evaluated, so that this artifact is nonexistent in the GSM. Consequently, the enhanced proton-proton correlations at the proton drip-line are very probably due to the confining effect of the Coulomb barrier. The important three-body effect would then be explained by the presence of the Coulomb interaction. Let us consider only the two-body part of the Hamiltonian to state this fact. As the two-body part of the nucleon-nucleon interaction is mostly attractive and the Coulomb interaction repulsive, the total matrix elements of the two-body part of the Hamiltonian are generally smaller in absolute value for protons than for neutrons. Consequently, the effect of three-body forces is comparatively larger for proton-rich nuclei than for neutron-rich nuclei. The replacement of three-body forces by a renormalized two-body interaction of simple form then appears to be too strong an approximation at the proton drip-line. Two methods have successfully tackled the three-body part of the nuclear Hamiltonian in the proton-rich region. The first method, used in Ref. [13] within many-body perturbation theory (MBPT), consists of calculating directly the one- and two-body parts of the three-body force using normal ordering. As the residual part of three-body forces is negligible [67], this method replaces the initial three-body force by a very close two-body operator, providing in particular with the induced monopole correction [63]. The second method, utilized in Ref. [25] and this paper, consists in adding an A dependence

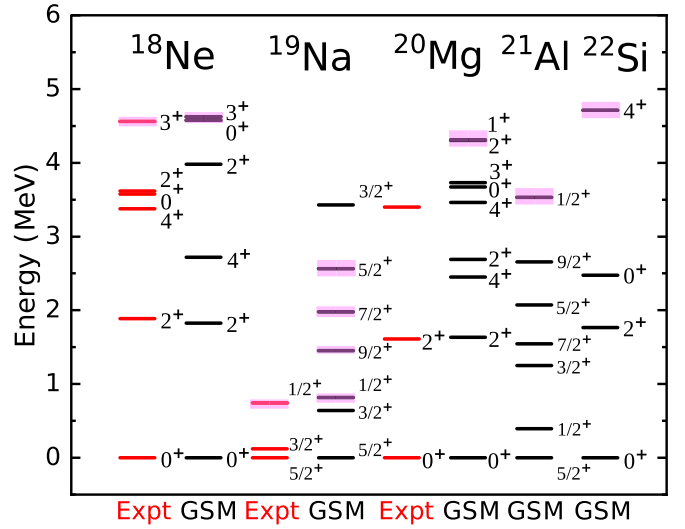


FIG. 4. Theoretical and experimental spectra of ^{16}O isotones for $A = 18$ – 22 . Energies are given in MeV. Proton-emission widths, also given in MeV, are represented by shaded areas. Theoretical energies and widths have been calculated with the GSM by using the A -dependent EFT interaction. Experimental data come from Refs. [13,66,68–70].

to the one-body and two-body parts of the Hamiltonian. It is indeed equivalent to monopole correction [62].

The spectra of proton-rich nuclei from ^{18}Ne to ^{22}Si , obtained using the EFT interaction in the GSM, are depicted in Fig. 4 along with available experimental data. The spectrum of ^{18}Ne is qualitatively well described, considering that it bears only two valence protons. Indeed, the energy of the 2_1^+ state is very well reproduced. Its 4_1^+ , 2_2^+ , and 3_1^+ excited states differ from experimental data by a few hundreds of keV at most, while the calculated 0_2^+ excited state is too high in energy by about 1 MeV. The spectrum of ^{19}Na is of the same quality, as the energy of the $1/2_1^+$ state is very close to experimental data, while that of the $3/2_1^+$ state is too low by about 500 keV. The spectra of the same nuclei obtained with MBPT in Ref. [13] are comparable. Indeed, while the energy of the 4_1^+ state of ^{18}Ne is closer to experiment therein, that of the 2_2^+ state of ^{18}Ne is about 1 MeV too low. The GSM calculation of the first-excited state of ^{20}Mg , of 2^+ character, compares well with experiment. The second-excited state of ^{20}Mg , predicted to be a 4^+ state in Ref. [71], would be too low with the GSM, similarly to that of ^{18}Ne . The spectra of ^{21}Al and ^{22}Si , not known experimentally, can be compared with those obtained in Ref. [13]. Our first-excited states are in the same order, except for the $7/2_1^+$ state of ^{21}Al , slightly lower in our case. Hence, the comparison of our GSM results with experimental data, on the one hand, and the theoretical calculations of Ref. [13], done with the realistic framework of MBPT, on the other hand, showed that the GSM Hamiltonian can provide with physically sound excited states. The spectra provided by the FHT interaction do not compare well with experimental data, however, so that they are not shown. Consequently, one can properly estimate the Coulomb contribution of the Hamiltonian to the excited

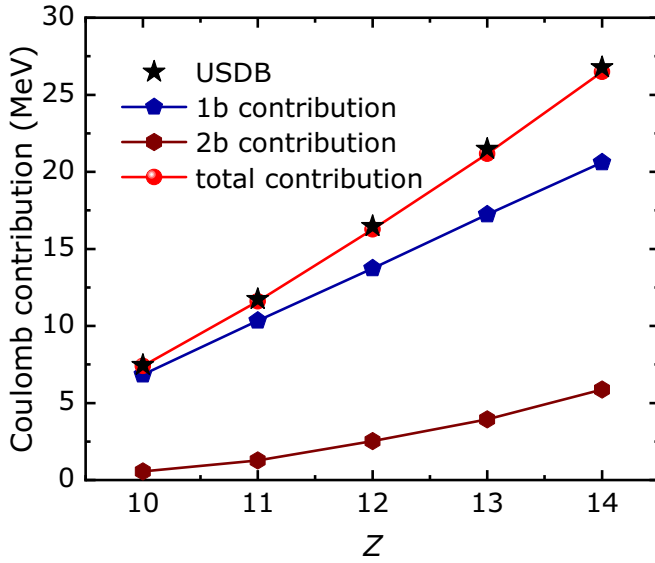


FIG. 5. Hamiltonian Coulomb contributions (in MeV) of the ground states of ^{16}O isotones as a function of their proton number Z . Solid lines are issued from a GSM calculation using the A -dependent EFT interaction. Stars point out the IMME Coulomb energies [40–42]. The GSM results shown consist of the ^{16}O core Coulomb one-body part (1b contribution), of the valence Coulomb two-body part (2b contribution), and of their sum (total contribution). Solid lines are present only to guide the eye.

states by using the A -dependent EFT interaction and compare it with that effected in other theoretical models. We will also only consider the A -dependent EFT interaction with the GSM afterwards.

IV. COULOMB CONTRIBUTIONS

The Coulomb contributions, i.e., the expectations values of the one-body, two-body, and total Coulomb Hamiltonians, are depicted in Fig. 5 for the ground states of ^{16}O isotones from ^{18}Ne to ^{22}Si , and in Figs. 6 and 7 for the spectra of ^{18}Ne and ^{20}Mg , respectively. The IMME formula used along with the USDB interaction should depend in principle on angular momentum and state number [41]. However, in practice, the IMME values are a function of isospin only [41], so that they are equal for all the Hamiltonian eigenstates of a fixed nucleus when using only proton valence states (see Figs. 6 and 7). In Fig. 5, one can see that the Coulomb contributions follow the usual rules present in closed quantum systems. Indeed, its one-body part grows linearly with the number of protons, while its two-body part has a quadratic increase. Moreover, the total Coulomb contribution is almost equal to the IMME value. This phenomenon is consistent with the observation done in the previous section when considering odd-even staggering and densities, i.e., that the Coulomb Hamiltonian has a tendency to confine valence protons inside the nuclear zone even if wave functions are unbound. The IMME formula is no longer suitable for excited states, however (see Figs. 6 and 7). Indeed, the total Coulomb contribution differs by several hundreds of keV to more than 1 MeV when going

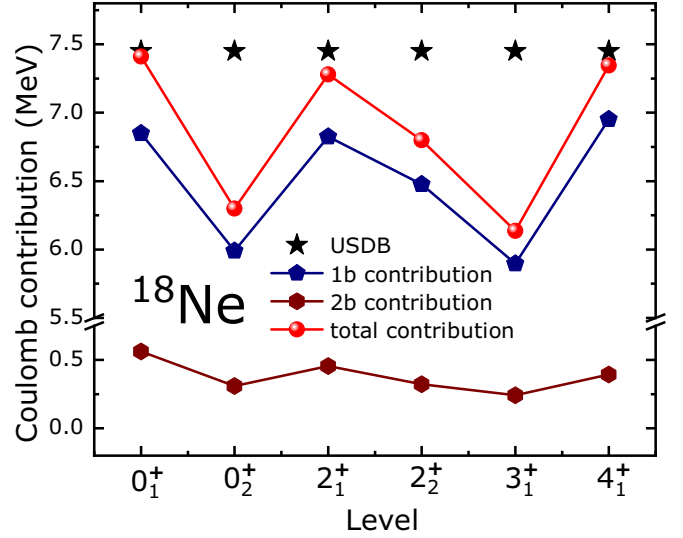


FIG. 6. Same as Fig. 5, but for the ground state and excited states of ^{18}Ne calculated with the GSM using the A -dependent EFT interaction (see Fig. 4).

from the ground states to neighboring excited states. In ^{18}Ne (see Fig. 6), while the first three states of the spectrum have a comparable Coulomb energy, it is smaller by 0.7 to 1.5 MeV in higher excited states. As all states lying above the 4_1^+ state in ^{18}Ne are unbound, one can infer that the drop in Coulomb energy might be due to the larger extension of these states. This fact is corroborated by the asymptotic behavior of the radial densities of the different states of the spectrum of ^{18}Ne and ^{20}Mg (see Figs. 8 and 9). Indeed, the Coulomb contribution is the smallest for the most extended states, which are the highest in the spectrum as well (see Fig. 4). One can note that the 2_2^+ states of ^{18}Ne and ^{20}Mg are intermediate between well-bound and well-unbound states

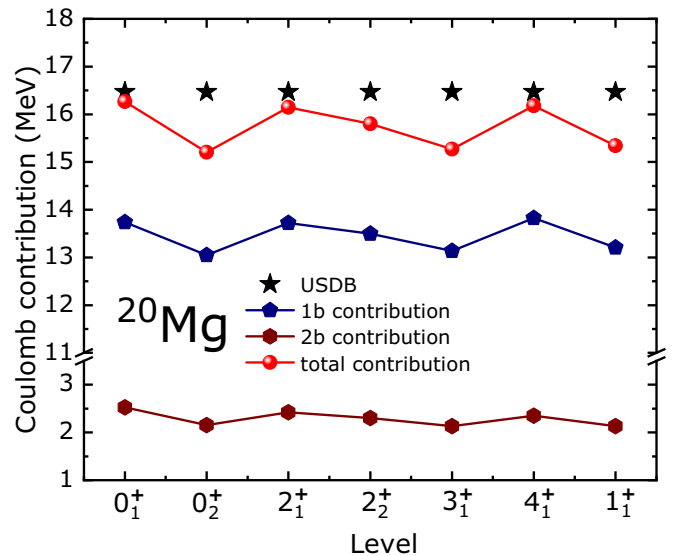


FIG. 7. Same as Fig. 6, but for the ground state and first-excited states of ^{20}Mg (see Fig. 4).

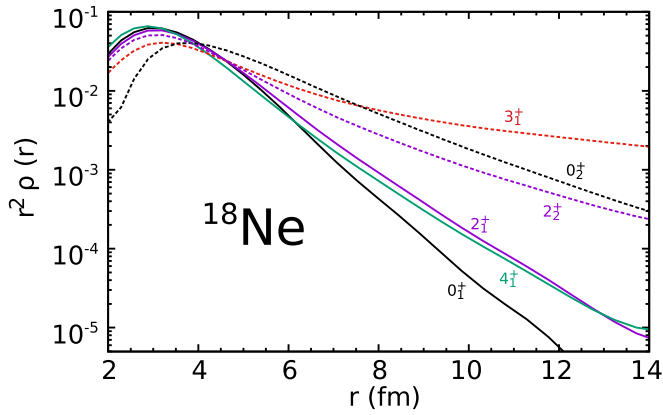


FIG. 8. Same as Fig. 3, but for the ground state and excited states of ^{18}Ne calculated with the GSM using the A -dependent EFT interaction (see Fig. 4). The bound and unbound states of the spectrum of ^{18}Ne are represented with solid and dashed lines, respectively.

(see Fig. 9). This translates into a 2_2^+ Coulomb contribution which is halfway between those of the well-bound and -unbound states of considered nuclei (see Figs. 6 and 7). Continuum coupling is thus necessary to properly account for the slow decay of unbound states in the medium asymptotic region. Moreover, one can see that the one-body part of the Coulomb Hamiltonian is dominant, its two-body part only adding a value around 200 to 500 keV for ^{18}Ne (see Fig. 6). Nevertheless, the pattern followed by the one-body and two-body parts of the Coulomb contribution is the same. For example, the Coulomb contribution of both parts decreases when going from the 0_1^+ state to the 0_2^+ state and augments from the 0_2^+ state to the 2_1^+ state (see Fig. 6). Consequently, the very different Coulomb contributions are mainly due to the Coulomb interaction of the valence protons with the core. The situation is qualitatively similar in ^{20}Mg for the total Coulomb contributions (see Fig. 7), because Coulomb energies differ by 0.5 to 1 MeV. One can note that the one-body and two-body parts of the expectation values of the Coulomb Hamiltonian are typically two and four times larger than in ^{18}Ne . It was to

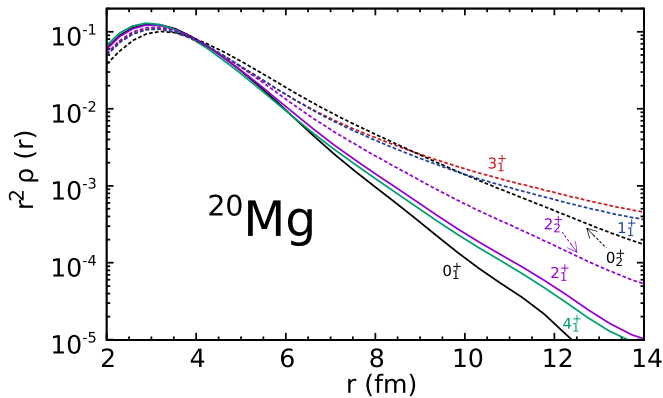


FIG. 9. Same as Fig. 8, but for the ground state and first-excited states of ^{20}Mg calculated with the GSM using the A -dependent EFT interaction (see Fig. 4).

be expected because ^{18}Ne and ^{20}Mg have two and four valence protons, respectively. The contributions of the Coulomb one-body and two-body parts also follow the same pattern in ^{20}Mg as that described in ^{18}Ne (see Figs. 6 and 7). However, the two-body Coulomb expectation values in ^{20}Mg exhibits larger differences than in ^{18}Ne , so that the variations of the total Coulomb contribution are more pronounced than those of its one-body part. As a consequence, we could show that the IMME formula, devised from isobaric analog states near the valley of stability, is justified only for ground states. Indeed, excited states well above the proton-emission threshold do not follow this rule. The precise calculation of Coulomb contributions for the proton drip-line nuclei thus demands the inclusion of continuum coupling in general. The GSM is thus a better tool for that purpose than the HO-SM.

V. ELASTIC SCATTERING CROSS SECTIONS OF THE $^{18}\text{Ne}(p, p)$ REACTION

To test the predictive power of our approach, we calculated a reaction observable, which is not included in the fitting procedure. The calculation of reaction observables is indeed meaningful for experimental studies; for example, to better understand nuclear astrophysics experimental data [73]. The GSM has thus been supplemented recently by the resonating group method (RGM) [74], so that cross sections can be calculated therein. The most recent applications concern deuteron elastic scattering [50] as well as radiative capture [48,49]. The excitation functions arising from the $^{18}\text{Ne}(p, p)$ reaction are of significant interest because experimental data have been measured at several low-lying energies. Moreover, these excitation functions depend on the unbound spectrum of ^{19}Na , so that structure degrees of freedom must be properly included in order to precisely reproduce experimental data. The excitation functions of the $^{18}\text{Ne}(p, p)$ reaction had already been calculated in the GSM-RGM [74]. However, a phenomenological Hamiltonian, fit on the binding energy and spectra of ^{18}Ne and ^{19}Na only was used therein. Indeed, the aim of Ref. [74] was mainly to demonstrate the feasibility of the GSM-RGM calculations. The situation is thus different because the GSM Hamiltonian used is fit on ^{16}O isotones up to ^{22}Si , so that the quality of excitation functions is a direct measure of the ability of the EFT interaction to effectively reproduce experimental data. The excitation functions of the $^{18}\text{Ne}(p, p)$ reaction obtained from the GSM-RGM are shown in Fig. 10. One can see that experimental data are well described. The sudden increase of the excitation function, due to the $1/2_1^+$ excited state of ^{19}Na , is in particular well reproduced. However, one can notice a slight shift of the calculated excitation functions compared with experimental data if the angle is equal to 120.2 or 156.6 degrees (see Fig. 10). In fact, it would have been necessary to fit the spectra of ^{18}Ne and ^{19}Na up to a few keV to match experimental data almost exactly, as was done in Ref. [74]. The experimental data of the considered excitation functions are then properly reproduced for all projectile energies. Consequently, the GSM can make efficient predictions of reaction observables starting from a Hamiltonian fit from structure only.

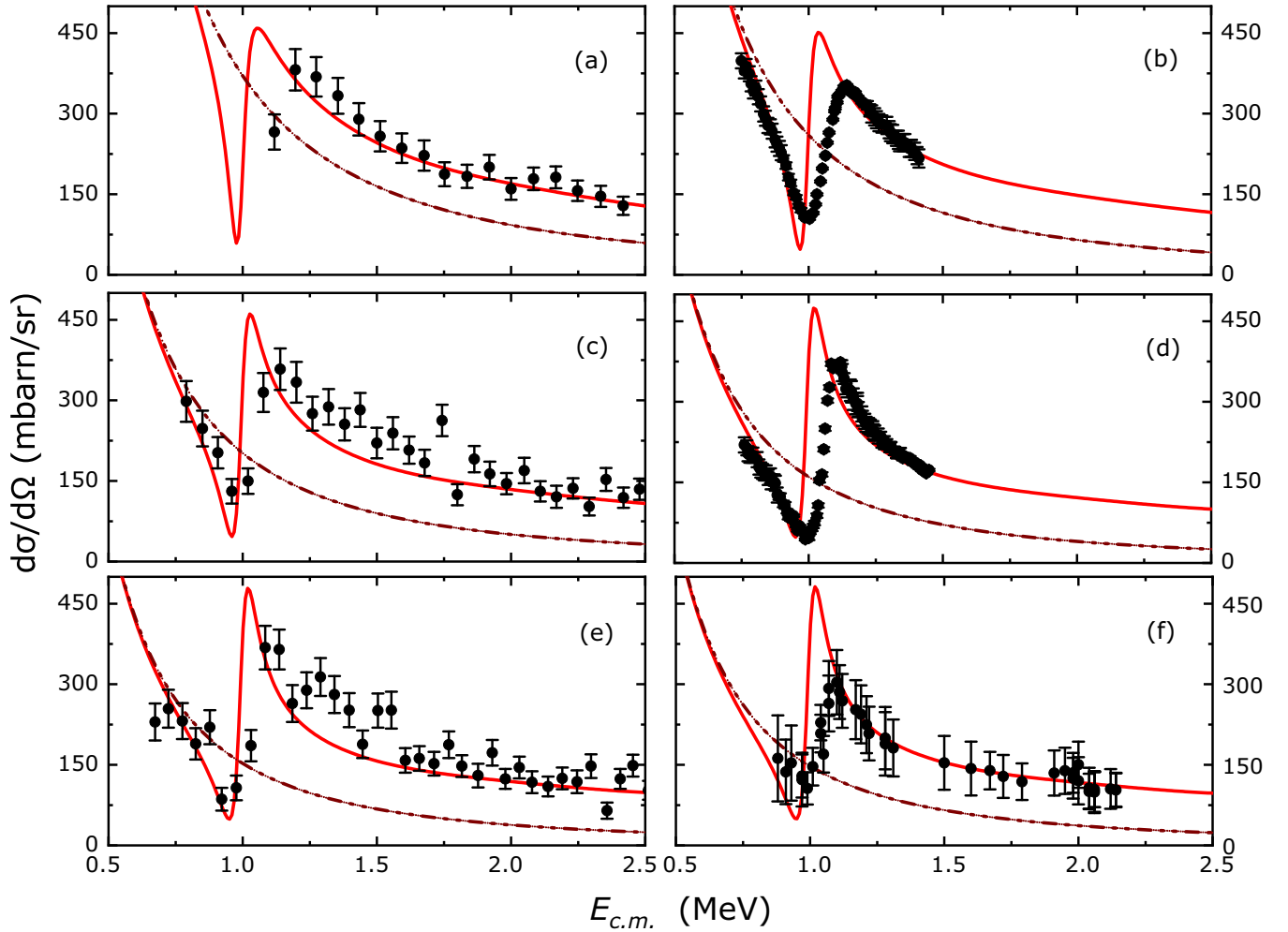


FIG. 10. Excitation functions of the $^{18}\text{Ne}(p, p)$ reaction, denoted $d\sigma/d\Omega$ (mbarn/sr), as a function of the proton-projectile center-of-mass energy $E_{c.m.}$ (in MeV). Panels (a)–(f) respectively depict excitation functions considered at a center-of-mass angle equal to 105, 120.2, 135, 156.6, 165, and 180 degrees. Solid lines correspond to the results obtained with the GSM-RGM using the A -dependent EFT interaction; dashed lines represent pure Coulomb scattering excitation functions, and experimental data, taken from Refs. [68,72], are shown with filled circles.

VI. CONCLUSION

The need for continuum coupling might seem less important for the study of nuclei at the proton drip-line than for neutron-rich nuclei. Indeed, due to the presence of the Coulomb barrier, which confines protons in the nuclear region, the wave functions of proton-rich nuclei are expected to resemble those of closed quantum systems. Moreover, the unbound states of proton-rich nuclei in the medium and heavy regions of the nuclear chart bear lifetimes of the order of milliseconds, so that continuum effects are small therein. However, light proton-rich nuclei can exhibit phenomena usually arising only at the neutron drip-line, such as halos and resonance character at the ground-state level.

The ^{16}O isotones are particularly interesting for that matter because the Coulomb barrier is hereby rather important, while peculiarities associated with a sizable continuum coupling still occur. Hence, ^{16}O isotones have been studied by using the GSM so that the importance of continuum coupling could be precisely assessed, while the complex nature of internucleon

correlations has been handled via the use of two different effective two-body interactions in the presence or absence of A dependence. The most striking feature seen in ^{16}O isotones is the importance of three-body forces or, equivalently, A dependence of the two-body interaction used. While a phenomenological two-body force is sufficient to describe oxygen isotopes at the neutron drip-line, leading to an error of at most 500 keV, a discrepancy of several MeVs has been found to occur in ^{16}O isotones compared with experimental data if the effects of three-body forces are neglected. As the total two-body matrix elements of the Hamiltonian are the sum of nuclear and Coulomb parts, it is reasonable to assume that they are typically smaller in absolute value than in the neutron-rich region, where the nuclear interaction dominates. As a consequence, the relative importance of three-body forces is larger. In fact, either a very precise equivalent two-body operator, arising from the normal ordering method [67], or an explicit use of A dependence, as done in this work, could provide with a good reproduction of the three-body force effects. Moreover, while the FHT interaction could reproduce

ground states fairly well, the spectra obtained therein were not satisfactory, contrary to the EFT interaction. The closer relation of the EFT interaction to realistic nucleon-nucleon interaction might be the reason for that state of affairs, as the FHT interaction is local and, hence, more phenomenological than the EFT interaction. Indeed, as noted earlier, the partial cancellation of nuclear and Coulomb parts in matrix elements might also enhance the nonlocal effects of the nuclear interaction, thus preventing a good description of ^{16}O isotones with a local interaction, contrary to neutron-rich oxygen isotopes.

The importance of continuum coupling in ^{16}O isotones could be quantitatively studied. While the ground states of ^{16}O isotones are mainly localized in the nuclear region, even when they are unbound, the proton densities of their excited states bear sizable asymptotes. This generated an interesting pattern in Coulomb contributions because those associated with the ground states of ^{16}O isotones follow the IMME prescription, while those of unbound excited states depart from those values by a few MeVs due to continuum coupling. Consequently, continuum coupling has to be included if one aims at studying proton-rich nuclei in the $A \approx 20$ region, even if the Coulomb barrier is rather strong therein. While the ground states of ^{16}O isotones can be satisfactorily described by closed quantum systems, even when they are of resonance character, this is not the case for their excited states. Only a proper inclu-

sion of continuum coupling can allow us to discriminate between localized and extended many-body states at the proton drip-line.

The predictive character of the GSM has been tested by considering the excitation function of the $^{18}\text{Ne}(p, p)$ reaction. The Hamiltonian has been fit only from the structure properties of the spectra of ^{16}O isotones. The calculated excitation functions of the $^{18}\text{Ne}(p, p)$ reaction compare well with experimental data for all considered angles. It is, in particular, due to the good description of the $1/2_1^+$ excited state of ^{19}Na with the GSM, responsible from the fast increase of excitation functions close to $E_{c.m.} = 1$ MeV.

ACKNOWLEDGMENTS

This work has been supported by the National Natural Science Foundation of China under Grants No. 11435014, No. 11835001, No. 11921006, No. 11847203, and No. 11975282; the National Key R&D Program of China under Grant No. 2018YFA0404401; and the CUSTIPEN (China-U.S. Theory Institute for Physics with Exotic Nuclei) funded by the U.S. Department of Energy, Office of Science under Grant No. sc0009971. We acknowledge the High-Performance Computing Platform of Peking University for providing computational resources.

-
- [1] I. Tanihata, H. Savajols, and R. Kanungo, *Prog. Part. Nucl. Phys.* **68**, 215 (2013).
 - [2] T. Motobayashi, *EPJ Web Conf.* **66**, 01013 (2014).
 - [3] B. Blank and M. Borge, *Prog. Part. Nucl. Phys.* **60**, 403 (2008).
 - [4] M. Pfützner, M. Karny, L. V. Grigorenko, and K. Riisager, *Rev. Mod. Phys.* **84**, 567 (2012).
 - [5] M. Wang, G. Audi, F. Kondev, W. Huang, S. Naimi, and X. Xu, *Chin. Phys. C* **41**, 030003 (2017).
 - [6] L. Gaudefroy, W. Mittig, N. A. Orr, S. Varet, M. Chartier, P. Roussel-Chomaz, J. P. Ebran, B. Fernández-Domínguez, G. Frémont, P. Gangnant *et al.*, *Phys. Rev. Lett.* **109**, 202503 (2012).
 - [7] T. Baumann, A. Amthor, D. Bazin, B. Brown, C. Folden III, A. Gade, T. Ginter, M. Hausmann, M. Matoš, D. Morrissey *et al.*, *Nature (London)* **449**, 1022 (2007).
 - [8] H. L. Crawford, P. Fallon, A. O. Macchiavelli, P. Doornenbal, N. Aoi, F. Browne, C. M. Campbell, S. Chen, R. M. Clark, M. L. Cortés *et al.*, *Phys. Rev. Lett.* **122**, 052501 (2019).
 - [9] M. Thoennessen, *Prog. Theor. Phys. Suppl.* **67**, 193 (2004).
 - [10] H. B. Yang, L. Ma, Z. Y. Zhang, C. L. Yang, Z. G. Gan, M. M. Zhang, M. H. Huang, L. Yu, J. Jiang, Y. L. Tian *et al.*, *Phys. Lett. B* **777**, 212 (2018).
 - [11] Y. T. Oganessian, V. K. Utyonkov, Y. V. Lobanov, F. S. Abdullin, A. N. Polyakov, R. N. Sagaidak, I. V. Shirokovsky, Y. S. Tsyganov, A. A. Voinov, G. G. Gulbekian *et al.*, *Phys. Rev. C* **74**, 044602 (2006).
 - [12] J. R. Brown, M. A. Bentley, P. Adrich, D. Bazin, J. M. Cook, C. A. Diget, A. Gade, T. Glasmacher, S. M. Lenzi, S. McDaniel *et al.*, *Phys. Rev. C* **80**, 011306(R) (2009).
 - [13] J. D. Holt, J. Menéndez, and A. Schwenk, *Phys. Rev. Lett.* **110**, 022502 (2013).
 - [14] J. Park, R. Krücken, D. Lubos, R. Gernhäuser, M. Lewitowicz, S. Nishimura, D. S. Ahn, H. Baba, B. Blank, A. Blazhev *et al.*, *Phys. Rev. C* **99**, 034313 (2019).
 - [15] S. Åberg, P. B. Semmes, and W. Nazarewicz, *Phys. Rev. C* **56**, 1762 (1997); **58**, 3011(E) (1998).
 - [16] A. T. Kruppa, B. Barmore, W. Nazarewicz, and T. Vertse, *Phys. Rev. Lett.* **84**, 4549 (2000).
 - [17] B. Barmore, A. T. Kruppa, W. Nazarewicz, and T. Vertse, *Phys. Rev. C* **62**, 054315 (2000).
 - [18] J. Al-Khalili, An Introduction to Halo Nuclei, in *The Euroschool Lectures on Physics with Exotic Beams*, edited by J. Al-Khalili and E. Roeckl (Springer, Berlin, Heidelberg, 2004), Vol. I, pp. 77–112.
 - [19] J. Giovannazzo, B. Blank, M. Chartier, S. Czajkowski, A. Fleury, M. J. Lopez Jimenez, M. S. Pravikoff, J.-C. Thomas, F. de Oliveira Santos, M. Lewitowicz *et al.*, *Phys. Rev. Lett.* **89**, 102501 (2002).
 - [20] C. Dossat, A. Bey, B. Blank, G. Cachel, A. Fleury, J. Giovannazzo, I. Matea, F. de Oliveira Santos, G. Georgiev, S. Grévy *et al.*, *Phys. Rev. C* **72**, 054315 (2005).
 - [21] J. Rotureau, J. Okołowicz, and M. Płoszajczak, *Nucl. Phys. A* **767**, 13 (2006).
 - [22] N. Michel, W. Nazarewicz, M. Płoszajczak, and K. Bennaceur, *Phys. Rev. Lett.* **89**, 042502 (2002).
 - [23] K. Fosse, J. Rotureau, N. Michel, and W. Nazarewicz, *Phys. Rev. C* **96**, 024308 (2017).
 - [24] N. Michel, W. Nazarewicz, M. Płoszajczak, and T. Vertse, *J. Phys. G* **36**, 013101 (2009).
 - [25] F. De Grancey *et al.*, *Phys. Lett. B* **758**, 26 (2016).
 - [26] M. D. Jones, K. Fosse, T. Baumann, P. A. DeYoung, J. E. Finck, N. Frank, A. N. Kuchera, N. Michel, W. Nazarewicz, J. Rotureau *et al.*, *Phys. Rev. C* **96**, 054322 (2017).

- [27] S. Leblond, F. M. Marqués, J. Gibelin, N. A. Orr, Y. Kondo, T. Nakamura, J. Bonnard, N. Michel, N. L. Achouri, T. Aumann *et al.*, *Phys. Rev. Lett.* **121**, 262502 (2018).
- [28] G. Papadimitriou, J. Rotureau, N. Michel, M. Płoszajczak, and B. R. Barrett, *Phys. Rev. C* **88**, 044318 (2013).
- [29] Z. Sun, Q. Wu, Z. Zhao, B. Hu, S. Dai, and F. Xu, *Phys. Lett. B* **769**, 227 (2017).
- [30] B. S. Hu, Q. Wu, Z. H. Sun, and F. R. Xu, *Phys. Rev. C* **99**, 061302(R) (2019).
- [31] C. R. Hoffman, T. Baumann, D. Bazin, J. Brown, G. Christian, P. A. DeYoung, J. E. Finck, N. Frank, J. Hinnefeld, R. Howes, P. Mears *et al.*, *Phys. Rev. Lett.* **100**, 152502 (2008).
- [32] P. Doornenbal, H. Scheit, S. Takeuchi, Y. Utsuno, N. Aoi, K. Li, M. Matsushita, D. Steppenbeck, H. Wang, H. Baba *et al.*, *Phys. Rev. C* **95**, 041301(R) (2017).
- [33] C. Caesar *et al.* (R3B Collaboration), *Phys. Rev. C* **88**, 034313 (2013).
- [34] J. D. Holt, J. Menéndez, and A. Schwenk, *Eur. Phys. J. A* **49**, 39 (2013).
- [35] G. Hagen, M. Hjorth-Jensen, G. R. Jansen, R. Machleidt, and T. Papenbrock, *Phys. Rev. Lett.* **108**, 242501 (2012).
- [36] J. B. Ehrman, *Phys. Rev.* **81**, 412 (1951).
- [37] R. G. Thomas, *Phys. Rev.* **88**, 1109 (1952).
- [38] T. Otsuka, T. Suzuki, J. D. Holt, A. Schwenk, and Y. Akaishi, *Phys. Rev. Lett.* **105**, 032501 (2010).
- [39] N. Michel, *Phys. Rev. C* **83**, 034325 (2011).
- [40] J. Britz, A. Pape, and M. S. Antony, *At. Data Nucl. Data Tables* **69**, 125 (1998).
- [41] W. E. Ormand, *Phys. Rev. C* **55**, 2407 (1997).
- [42] B. A. Brown and W. A. Richter, *Phys. Rev. C* **74**, 034315 (2006).
- [43] H. Furutani, H. Horiuchi, and R. Tamagaki, *Prog. Theor. Phys.* **62**, 981 (1979).
- [44] H. Furutani, H. Kanada, T. Kaneko, S. Nagata, H. Nishioka, S. Okabe, S. Saito, T. Sakuda, and M. Seya, *Prog. Theor. Phys. Suppl.* **68**, 193 (1980).
- [45] R. Machleidt and D. Entem, *Phys. Rep.* **503**, 1 (2011).
- [46] K. Fosse, J. Rotureau, N. Michel, Q. Liu, and W. Nazarewicz, *Phys. Rev. C* **94**, 054302 (2016).
- [47] Y. Jaganathen, R. M. Id Betan, N. Michel, W. Nazarewicz, and M. Płoszajczak, *Phys. Rev. C* **96**, 054316 (2017).
- [48] K. Fosse, N. Michel, M. Płoszajczak, Y. Jaganathen, and R. M. Id Betan, *Phys. Rev. C* **91**, 034609 (2015).
- [49] G. X. Dong, N. Michel, K. Fosse, M. Płoszajczak, Y. Jaganathen, and R. M. Id Betan, *J. Phys. G* **44**, 045201 (2017).
- [50] A. Mercenne, N. Michel, and M. Płoszajczak, *Phys. Rev. C* **99**, 044606 (2019).
- [51] T. Berggren, *Nucl. Phys. A* **109**, 265 (1968).
- [52] R. Newton, *Scattering Theory of Waves and Particles*, 2nd ed. (Dover Publications, New York, 2013).
- [53] G. J. G. Sleijpen and H. A. van der Vorst, *SIAM J. Matrix Anal. Appl.* **17**, 401 (1996).
- [54] J. Rotureau, N. Michel, W. Nazarewicz, M. Płoszajczak, and J. Dukelsky, *Phys. Rev. Lett.* **97**, 110603 (2006).
- [55] J. Rotureau, N. Michel, W. Nazarewicz, M. Płoszajczak, and J. Dukelsky, *Phys. Rev. C* **79**, 014304 (2009).
- [56] N. Michel, W. Nazarewicz, M. Płoszajczak, and J. Okołowicz, *Phys. Rev. C* **67**, 054311 (2003).
- [57] N. Michel, *Comput. Phys. Commun.* **176**, 232 (2007).
- [58] N. Michel, W. Nazarewicz, and M. Płoszajczak, *Phys. Rev. C* **82**, 044315 (2010).
- [59] I. Talmi, *Helv. Phys. Acta* **25**, 185 (1952).
- [60] M. Moshinsky, *Nucl. Phys.* **13**, 104 (1959).
- [61] L. Huth, V. Durant, J. Simonis, and A. Schwenk, *Phys. Rev. C* **98**, 044301 (2018).
- [62] A. P. Zuker, *Phys. Rev. Lett.* **90**, 042502 (2003).
- [63] J. Duflo and A. P. Zuker, *Phys. Rev. C* **59**, R2347 (1999).
- [64] A. Bohr and B. Mottelson, *Nuclear Structure* (World Scientific Pub Co Inc, Singapore, New Jersey, London, Hong Kong, 1998).
- [65] B. A. Brown and B. H. Wildenthal, *Annu. Rev. Nucl. Part. Sci.* **38**, 29 (1988).
- [66] <http://www.nndc.bnl.gov/ensdf>.
- [67] G. Hagen, T. Papenbrock, D. J. Dean, A. Schwenk, A. Nogga, M. Włoch, and P. Piecuch, *Phys. Rev. C* **76**, 034302 (2007).
- [68] C. Angulo, G. Tabacaru, M. Couder, M. Gaelens, P. Leleux, A. Ninane, F. Vanderbist, T. Davinson, P. J. Woods, J. C. Schweitzer *et al.*, *Phys. Rev. C* **67**, 014308 (2003).
- [69] I. Mukha, K. Sümmerer, L. Acosta, M. A. G. Alvarez, E. Casarejos, A. Chatillon, D. Cortina-Gil, I. A. Egorova, J. M. Espino, A. Fomichev *et al.*, *Phys. Rev. C* **82**, 054315 (2010).
- [70] A. Gade, P. Adrich, D. Bazin, M. D. Bowen, B. A. Brown, C. M. Campbell, J. M. Cook, T. Glasmacher, K. Hosier, S. McDaniel *et al.*, *Phys. Rev. C* **76**, 024317 (2007).
- [71] J. S. Randhawa, R. Kanungo, M. Holl, J. D. Holt, P. Navrátil, S. R. Stroberg, G. Hagen, G. R. Jansen, M. Alcorta, C. Andreoiu *et al.*, *Phys. Rev. C* **99**, 021301(R) (2019).
- [72] F. de Oliveira Santos, P. Himpe, M. Lewitowicz, I. Stefan, N. Smirnova, N. L. Achouri, J. C. Angélique, C. Angulo, L. Axelsson, D. Baiborodin *et al.*, *Eur. Phys. J. A* **24**, 237 (2005).
- [73] I. J. Thompson and F. M. Nunes, *Nuclear Reactions for Astrophysics: Principles, Calculation and Applications of Low-Energy Reactions* (Cambridge University Press, Cambridge, UK, New York, 2009).
- [74] Y. Jaganathen, N. Michel, and M. Płoszajczak, *Phys. Rev. C* **89**, 034624 (2014).